Topological valley transport of gapped Dirac magnons in bilayer ferromagnetic insulators

Zhai, Xuechao; Blanter, Yaroslav M.

DOI
10.1103/PhysRevB.102.075407

Publication date
2020

Document Version
Final published version

Published in
Physical Review B

Topological valley transport of gapped Dirac magnons in bilayer ferromagnetic insulators

Xuechao Zhai[1,2,*] and Yaroslav M. Blanter[2,†]

[1]*New Energy Technology Engineering Laboratory of Jiangsu Province & Institute of Information Physics, School of Science, Nanjing University of Posts and Telecommunications (NJUPT), Nanjing 210023, China*

[2]*Kavli Institute of NanoScience, Delft University of Technology, 2628 CJ Delft, The Netherlands*

(Received 25 February 2020; revised 8 July 2020; accepted 24 July 2020; published 4 August 2020)

Bilayer Heisenberg ferromagnetic insulators hold degenerate terahertz Dirac magnon modes associated with two opposite valleys of the hexagonal Brillouin zone. We show that this energy degeneracy can be removed by breaking of the inversion symmetry ($\mathcal{I}$), leading to a topological magnon valley current. We show furthermore that this current leads to valley Seebeck effect for magnons and is thereby detectable. We perform calculations in the specific example of bilayer $CrBr_3$, where $\mathcal{I}$ can be broken by electrostatic doping.

DOI: 10.1103/PhysRevB.102.075407

I. INTRODUCTION

Recent discoveries of atomic-thick ferromagnetic (FM) insulators [1,2] represent a landmark for two-dimensional (2D) fundamental and applied physics. Stable long-range 2D FM order strongly relies on the presence of magnetic anisotropy [3–5]. In these materials magnons, elementary excitations of magnetic structure, usually have spectra with Dirac points. In particular, magnons in two of the most popular 2D FM insulators have been studied in more detail: gapless Dirac properties protected by inversion symmetry ($\mathcal{I}$) and time-reversal-and-rotational symmetry ($\mathcal{T}C_r$) in monolayer $CrBr_3$ [6] with no observable Dzyaloshinskii-Moriya interaction (DMI), and topological gaps induced by $\mathcal{T}C_r$ breaking due to the observable DMI in monolayer CrI_3 [7]. The operators $\mathcal{T}, C_r$ acting in real space indicate time reversal and π rotation around an in-plane symmetrical axis of the hexagonal lattice of localized spins, respectively. This symmetry analysis was previously clarified in theoretical models [8].

The graphenelike spectrum of 2D magnons is characterized by the appearance of two valleys K and K' of the hexagonal Brillouin zone. The valley index can serve as a quantum number [9–13], and it has been already demonstrated in electron systems [14,15], and more recently also in 2D photonic [16] and phononic [17] crystals that it can form a basis for quantum information transfer. However, it is very difficult to use the valley degree of freedom for 2D magnons. On one hand, the magnons near K (K') have large momentum and no charge, and thus the usual magnon manipulation methods such as FM resonance [18] or electric, magnetic, or optical methods [14–17] cannot easily detect the two valleys, not even speaking about their difference. On the other hand, the concept of Fermi energy is absent for bosonic magnons, and thus one can only thermally excite the (THz) valley magnons [19] simultaneously with other low-frequency modes.

Instead, in order to utilize the valley degree of freedom in 2D magnets, we turn to the concept of topology [8,20–24]. It is attractive since the topological magnon transport is insensitive to sample defects. The topological current is in principle dictated by the crystal symmetry [21–23], which is difficult to change in three-dimensional (3D) systems. The momentum-dependent topological magnon current, odd under $\mathcal{T}C_r$ but even under $\mathcal{I}$ [8,25,26], is strictly zero in pristine magnon systems respecting both $\mathcal{I}$ and $\mathcal{T}C_r$—typical FM Heisenberg systems [6,25]. However, if $\mathcal{I}$ is broken for magnons in FM insulators, $\mathcal{T}C_r$ requires the Hall current to have the opposite values in two valleys, resulting in a magnon valley Hall current, in analogy with electron systems [26–28]. The $\mathcal{I}$ breaking cannot be induced by the external electric field, since the localized moments do not change with the electric potential [29], however, it can be induced by layer-dependent electrostatic doping [30] in bilayer magnets.

In this work we explore the topological valley transport of magnons under $\mathcal{I}$ breaking in bilayer Heisenberg FM insulators. We propose that the pure magnon valley current can be detected via the inverse valley Hall effect, and discuss a concept of valley Seebeck effect for 2D magnets. We perform calculations for the specific example of bilayer $CrBr_3$ [31,32], where $\mathcal{I}$ of magnons ($\sim$1.8 THz near two valleys) can be broken by electrostatic doping. The results show how the valley degree of freedom can be manipulated in 2D magnets and opens the way of using it for information transfer—THz magnon valleytronics.

We organize the paper as follows. In Sec. II we introduce the system Hamiltonian and magnon bands. In Sec. III we show how to generate the topological magnon valley current. In Sec. IV we demonstrate how to detect the topological magnon valley transport. In Sec. V we show the material realization. In the final section we present the discussion and conclusions.

II. SYSTEM HAMILTONIAN AND MAGNON BANDS

We consider a bilayer collinear FM insulator on a usual AB-stacked honeycomb lattice with the magnetic anisotropy

*zxc@njupt.edu.cn
†Y.M.Blanter@tudelft.nl

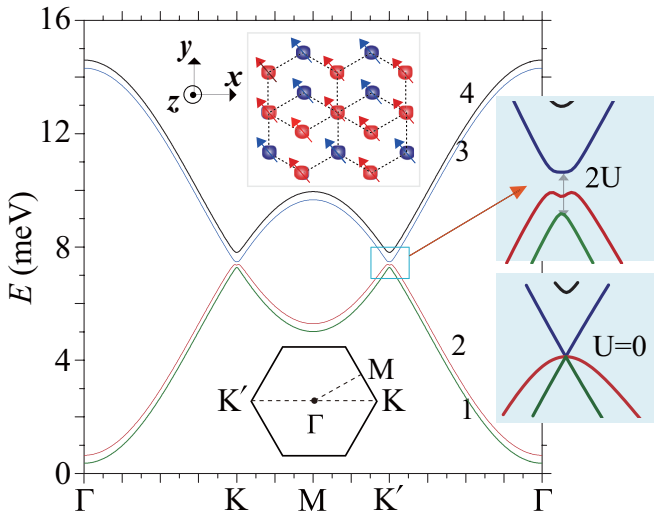

FIG. 1. Magnon spectrum of bilayer $CrBr_3$ with $J = 1.55$ meV, $J_z = 0.2$ meV, $S = 3/2$, $\lambda = 0.05J$, $a = 3.72$ Å, $d_z = 6.11$ Å [6,32,35,36], assuming $U = 0.1$ meV. The top (bottom) inset sketches the structure in real (reciprocal) space. The right inset enlarges the gapped Dirac bands near 7.5 meV $\simeq 1.8$ THz. (The case $U = 0$ is plotted for comparison.)

perpendicular to the hexagon plane, i.e., spins on $\mu = A\alpha$, $B\alpha$ sublattices in the ground state satisfy $\boldsymbol{S}_{A\alpha} = \boldsymbol{S}_{B\alpha} = S\hat{z}$, where $\alpha = \pm$ indicates the top (bottom) layer, see Fig. 1. A general Heisenberg Hamiltonian [3–7] with breaking of $\mathcal{I}$ reads

$$\hat{\mathcal{H}} = -\sum_{\langle i,j\rangle} J_{ij}\boldsymbol{S}_i \cdot \boldsymbol{S}_j - \lambda \sum_{\langle i,j\rangle} S_i^z S_j^z + \sum_i \alpha U \hat{z} \cdot \boldsymbol{S}_i. \quad (1)$$

The first term represents the magnetic exchange interaction with $J_{ij} = J\,(J_z) > 0$ for intralayer (interlayer) nearest-neighbor magnetic moments. The second term indicates the anisotropic FM exchange with $\lambda > 0$ [4]. The last term H_U indicates $\mathcal{I}$ breaking [discussed in Eq. (11)]. By applying low magnetic field, the FM ground state can be stabilized. The essential physics will not be altered when the second- or third-nearest-neighbor exchange interactions are included. In addition, it is intuitive to identify the symmetry of $\mathcal{T}C_r$ in real space. A rigorous approach to prove $\mathcal{T}C_r$ of the system requires expanding Eq. (1) to the quadratic order [8].

Neglecting the magnon-magnon interactions in Eq. (1), the Holstein-Primakoff (HP) transformation [6] reads $S_{i\mu}^+ \equiv S_{i\mu}^x + iS_{i\mu}^y \simeq \sqrt{2S}c_{i\mu}$, $S_{i\mu}^- \equiv S_{i\mu}^x - iS_{i\mu}^y \simeq \sqrt{2S}c_{i\mu}^\dagger$, $S_{i\mu}^z = S - c_{i\mu}^\dagger c_{i\mu}$. In the A+, B+, A−, B− basis, the Bloch Hamiltonian after HP transformation is expressed as

$$H_{\boldsymbol{k}} = S\begin{pmatrix} J_z+\gamma+U & -Jf_{\boldsymbol{k}} & 0 & -J_z \\ -Jf_{\boldsymbol{k}}^* & \gamma+U & 0 & 0 \\ 0 & 0 & \gamma-U & -Jf_{\boldsymbol{k}} \\ -J_z & 0 & -Jf_{\boldsymbol{k}}^* & J_z+\gamma-U \end{pmatrix}, \quad (2)$$

where $f_{\boldsymbol{k}} = \exp(-ik_y a/2)[2\cos(\sqrt{3}k_x a/2) + \exp(i3k_y a/2)]$ (a is the hexagon side length) and $\gamma = 3(J+\lambda)$.

We now introduce the Pauli matrices in the sublattice ($\boldsymbol{\sigma}$) and layer ($\boldsymbol{\tau}$) spaces, considering Aα and the top layer (Bα and the bottom layer) as an up (down) pseudospin, respectively. The index $\xi = \pm$ denotes two valleys K and K' at $(k_x, k_y) = [4\pi/(3\sqrt{3}a)](\pm 1, 0)$. Expanding Eq. (2) near K and K', we obtain the effective Hamiltonian as

$$H_{\boldsymbol{q}} = \begin{pmatrix} H_{\boldsymbol{q}}^K & 0 \\ 0 & H_{\boldsymbol{q}}^{K'} \end{pmatrix}, \quad H_{\boldsymbol{q}}^\xi = \tau_0 h_{\boldsymbol{q}}^\xi + U_\gamma \tau_0\sigma_0 + \frac{J_z S}{2}\Gamma, \quad (3)$$

where $\boldsymbol{q} \equiv \boldsymbol{k} - K\,(K')$, $U_\gamma \equiv (\gamma + \alpha U)S$, $h_{\boldsymbol{q}}^\xi = \hbar\upsilon(\xi q_x\sigma_x + q_y\sigma_y)$ with $\upsilon = (3a/2)JS$, and $\Gamma = \tau_0\sigma_0 + \tau_z\sigma_z - \tau_x\sigma_x + \tau_y\sigma_y$ with τ_0 (σ_0) describing the pseudospin identity matrix.

We notice that there are two kinds of descriptions for time-reversal symmetry of quantum magnets in the literature. One, used by Ref. [8], is to define $\mathcal{T}$ that can directly operate in lattice space of localized spins (as stated above). Another description [25,33] is to use $\hat{\mathcal{T}}$ that operates only in the Bogoliubov Hamiltonian (2) or (3). For the former, one can combine $\mathcal{T}C_r$ with the Heisenberg equation of motion to solve the problem of spin precession [8]. For the latter, an ordered state must be assumed [33] when only the properties of magnons (HP bosons, collective excitation) are considered, and then $\hat{\mathcal{T}}$ has a specific matrix form, similar to the one for fermion systems [34]. For magnons, the symmetry analysis performed by $\hat{\mathcal{T}}$ and $\mathcal{T}C_r$ from different perspectives [8,25] lead to the same results. For the system we study, $\hat{\mathcal{T}}$, which interchanges two valleys, is found as

$$\hat{\mathcal{T}} = \begin{pmatrix} 0 & \tau_z\sigma_z \\ \tau_z\sigma_z & 0 \end{pmatrix} C = \hat{\mathcal{T}}^{-1}, \quad (4)$$

where C is the operator of complex conjugation. The relation $\hat{\mathcal{T}}\mathcal{H}_{\boldsymbol{q}}\hat{\mathcal{T}}^{-1} = \mathcal{H}_{\boldsymbol{q}}$ confirms the time-reversal invariance of the Bogoliubov Hamiltonian, leading to the energetically degeneracy of two valleys. The relation $\hat{\mathcal{T}}^2 = 1$ just reflects the spinless properties of magnons. The complex-conjugate property of Bloch functions between two valleys further ensures the validity of $\hat{\mathcal{T}}$ [34].

For convenience, we set $\hbar = 1$, $\upsilon = 1$ below. For $U = 0$, the eigenvalues of Eq. (3) read $E_n^0 = \gamma S + \varepsilon_n^0$, where $n = 1$ to 4 indexes the subband. Two magnon modes in each valley are massless Dirac modes (Fig. 1), $\varepsilon_{1,3}^0 = \mp\boldsymbol{q}$, and the other two modes have a gap, $\varepsilon_{2,4}^0 = J_z S \mp [q^2 + (J_z S)^2]^{1/2}$. Therefore, a triple degeneracy [25] exists at $K\,(K')$ point ($q = 0$). For $U \neq 0$, the eigenvalues are $E_n = \gamma S + \varepsilon_n$, $\mathcal{I}$ is broken, the Dirac magnon subbands are gapped (Fig. 1), and the triplet degeneracy in each valley is lifted although the two valleys are energetically degenerate. In contrast, there is no counterpart of this model in 2D electron systems [11–15,37].

By using perturbation theories [38–40] under $U/J_z \ll 1$, we can find the eigenvalues ε_n as

$$\varepsilon_1 \simeq \frac{\Delta_-}{2} - \sqrt{2q^2\cos^2\frac{\varphi}{2} + \frac{\Delta_+^2}{4}},$$
$$\varepsilon_4 \simeq \varepsilon_4^0 + \frac{U^2 S}{2J_z}(2 - \cos\theta), \quad (5)$$

where $\Delta_\pm = [J_z - (J_z^2 + U^2)^{1/2} \pm U]S$, $\cos\varphi = U/(J_z^2 + U^2)^{1/2}$, $\cos\theta = J_z/(q^2 + J_z^2)^{1/2}$. Here $\varepsilon_{2,3}(q)$ are not presented due to their complexity (Supplemental Material

(SM) [40]). Specifically, the energies at K (K') read

$$\varepsilon^0_{1,3} = \mp US, \quad \varepsilon^0_{2,4} = \left(J_z \mp \sqrt{J_z^2 + U^2}\right)S, \tag{6}$$

agreeing with the numerical result in Fig. 1.

III. GENERATION OF TOPOLOGICAL MAGNON VALLEY CURRENT

We consider a rectangular sample with width W and length L. By applying energy-flux quantum theory [41–43] to noninteracting magnons, we obtain the average energy current density as

$$\boldsymbol{J}_\varepsilon = \frac{1}{2V}\sum_{\boldsymbol{k}} u^\dagger_{m\boldsymbol{k}}\left(\frac{\partial \mathcal{H}_{\boldsymbol{k}}}{\partial \boldsymbol{k}}^2\right)_{mn} u_{n\boldsymbol{k}}, \tag{7}$$

where $V = WLd_z$ (d_z is the thickness) is the sample volume, and $u_{n\boldsymbol{k}}$ is the Bloch wave function for the nth subband. Using the Kubo formula acting on $\boldsymbol{J}_\varepsilon$ [41], the thermal Hall conductivity of magnons can be derived as $\kappa_{xy} = -(k_B^2 T/\hbar V)\sum_{n\boldsymbol{k}} C_{n\boldsymbol{k}}\Omega_{n\boldsymbol{k}}$, where the sum is all over the first Brillouin zone, $C_{n\boldsymbol{k}} = (1+f_B)[\ln(1+1/f_B)]^2 - (\ln f_B)^2 - 2\mathrm{Li}_2(-f_B)$, with $f_B = [\exp(\varepsilon_{n\boldsymbol{k}}/k_B T) - 1]^{-1}$ denoting the Bose-Einstein distribution and Li_2 being the dilogarithm function. The Berry curvature here is determined by [26] $\boldsymbol{\Omega}_{n\boldsymbol{k}} \equiv \nabla_{\boldsymbol{k}} \times \langle u_{n\boldsymbol{k}}|i\nabla_{\boldsymbol{k}}|u_{n\boldsymbol{k}}\rangle = \Omega_{n\boldsymbol{k}}\hat{\boldsymbol{z}}$, where $\hat{\boldsymbol{z}}$ is the unit vector in the out-of-plane direction.

Because the magnonic system has $\hat{\mathcal{T}}$, the magnons near K and K' can feel the opposite orbit pseudomagnetic field reflected in $\Omega^K_{n\boldsymbol{q}} = -\Omega^{K'}_{n,-\boldsymbol{q}}$, as shown in Fig. 2. Our detailed

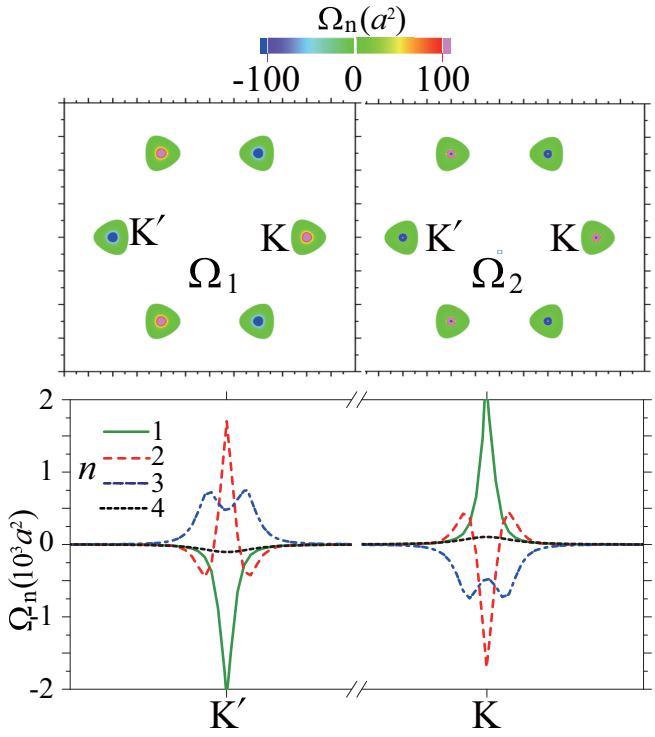

FIG. 2. Berry curvature in the (k_x, k_y) plane (top) and along the K'-K direction (bottom), corresponding to the gapped Dirac magnon band in Fig. 1.

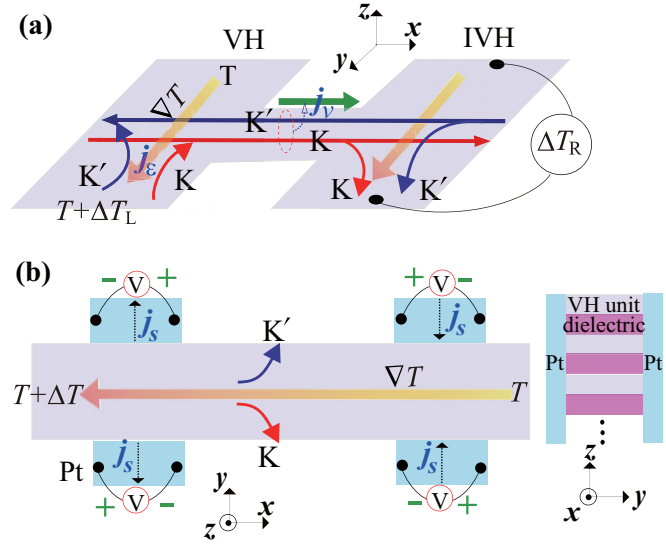

FIG. 3. (a) A Hall bar to thermally detect a net pure valley Hall (VH) current $\boldsymbol{j}_v$ via the inverse VH (IVH) effect, analogous to the detector for the electron case [15,21]. The valley Hall current along x direction comes from the left bar when magnon energy current $\boldsymbol{j}_\varepsilon$ flows along y direction and is detected on the right bar. (b) Left: A device of valley Seebeck effect for magnons. Inverse spin Hall (ISH) effect [44,46] occurs in Pt metallic contact (optionally), where $\boldsymbol{j}_s$ is the spin current. Right: A proposed valley-Seebeck integrated system composed of VH units separated by a nonmagnetic dielectric layer (e.g., layered boron nitride [30]). This setup is suggested to increase the measured signal.

calculations [40] reveal the local conservation law of the Berry curvature [26] $\sum_{n=1}^4 \Omega_{n\boldsymbol{k}} = 0$. We have $\kappa_{xy} = 0$ because the contributions from K and K' cancel each other, however, a pure valley current of magnons is generated. To distinguish the difference between K and K', it is necessary to define a magnon valley Hall conductivity as $\kappa^v_{xy} \equiv \kappa^K_{xy} - \kappa^{K'}_{xy}$. It has the form

$$\kappa^v_{xy} = -\frac{k_B^2 T}{\hbar V}\sum_{n\boldsymbol{q}} C_{n\boldsymbol{q}}\left(\Omega^K_{n\boldsymbol{q}} - \Omega^{K'}_{n\boldsymbol{q}}\right), \tag{8}$$

where the summation over $\boldsymbol{q}$ around valley K (K') runs over half of the first Brillouin zone. As we concern in Eq. (3), the pure valley transport occurs due to $\Omega^K_{n\boldsymbol{q}} = -\Omega^{K'}_{n,-q}$.

IV. DETECTION OF TOPOLOGICAL MAGNON VALLEY TRANSPORT

The signal of topological valley transport κ^v_{xy} can be detected via the inverse magnon valley Hall effect, as sketched in Fig. 3(a). For thermal magnon transport, the directly observable qualities are thermal flux density j_ε and temperature difference [41], e.g., ΔT_L and ΔT_R in Fig. 3(a). From the well-known Onsager relation [44], we define a nonlocal thermal resistivity as $\rho_{NL} \equiv \Delta T_R/j_\varepsilon$. By using the appropriate boundary conditions (SM [40]), we self-consistently derive ρ_{NL} as

$$\rho_{NL} \approx \frac{W}{2\ell_v}\frac{(\kappa^v_{xy})^2}{(\kappa_{xx})^3}\exp\left(-\frac{L}{\ell_v}\right), \tag{9}$$

where $\kappa_{xx} = j_\varepsilon/\Delta T_{\rm L}$ is the local thermal conductivity. Note that Eq. (9) recovers the formula known for spin or valley Hall systems for electrons [21,45].

We emphasize that the setup of Fig. 3(a) is specifically designed to measure the contribution of the valley Hall effect. Indeed, no signal can be detected along x direction for the pure magnon valley Hall current we focus on. This means that one can add a detection along x direction to exclude the normal thermal Hall effect of magnons. To exclude the contribution from phonons and electrons to the thermal Hall effect, we present the following argument. First, we can ignore the electron transport in the insulating regime. Beyond this regime, the electron contribution to the thermal Hall current can be excluded by adjusting the Fermi energy, because the band topology strongly depends on the Fermi energy [21,22]. Second, the contribution from phonons to the thermal Hall current is absent in ordinary materials (including 2D magnets concerned here) because the observable phonon Hall effect usually needs special interaction mechanisms [47]. Third, the contribution of electrons and phonons to κ_{xx} (not Hall current) may be comparable to that of magnons at low temperatures [40,43], but only brings about a certain reduction of $\rho_{\rm NL}$. (This has been taken into account in the estimates of Sec. V.) Thus, the contribution of the pure magnon valley Hall effect can be quantified by using the design of Fig. 3(a).

An alternative method to detect $\kappa_{xy}^{\rm v}$ is by using heat-to-charge conversion [44]. We propose a concept of valley Seebeck effect, as sketched in Fig. 3(b), where Pt contacts (optionally) are added to the sample, and magnons from K, K' accumulate at the opposite sides. Consequently, spin current $\boldsymbol{j}_s$ can be induced in Pt due to s-d interaction (SM [40]) at the FM insulator/Pt metal interface [44,46,48]. The inverse spin Hall (ISH) electric field in Pt is determined by

$$\boldsymbol{E}_{\rm ISH} = (\rho\theta_{\rm SH})\boldsymbol{j}_s \times \boldsymbol{s}, \tag{10}$$

where ρ and $\theta_{\rm SH}$ indicate the electric resistance and spin Hall angle of Pt, $\boldsymbol{s}$ is an out-of-plane spin polarization vector. The ISH voltage is in principle determined by [40] $V_{\rm ISH} \propto j_s \propto \Delta T \sinh(x/\lambda_m)$, where $x = 0$ is at the center of the $CrBr_3$ sample and λ_m is the magnon relaxation length. Because the temperature difference between electrons in Pt and magnons in a FM insulator changes sign if the Pt contact is moved from left to right in Fig. 3(b), j_s and the ISH voltage change signs accordingly [40,46]. In the absence of valley Seebeck effect in Fig. 3(b), we judge that the contributions from normal spin Seebeck effect to ISH signal along $+y$ and $-y$ directions should in principle cancel out each other (independent of x) due to the transport symmetry. In this case, the net magnon current is in x direction (along the temperature gradient), and no net magnon current in y direction is converted into spin current in Pt leads under $\partial T/\partial y = 0$ in the magnet. Unlike the usual 3D case [46], the transport in z direction for the ultrathin 2D case here is negligible.

We now discuss deeply the detection in Fig. 3(b) as follows. First, an ideal way to make this setup requires growing metal leads attaching at the boundary of the 2D system. By this means, one can truly detect the 2D in-plane transport (excluding the out-of-plane contribution). By contrast, the recent experimental setups [49,50] were mainly based on the up-down configurations of metal leads and thicker 2D magnets (sub-10 nm thick), but physically the out-of-plane spin pumping probably dominates. Second, the ISH voltage is proportional to $\theta_{\rm SH}$ according to Eq. (10). Due to the rather small thickness of the 2D magnet, $\theta_{\rm SH}$ might be very small if the usually thicker metal leads are used due to the size effect. This would be an obstacle to the detection of the 2D in-plane magnon transport, although making metal leads thin enough is not impossible (technically, it is very difficult). To overcome this problem, we suggest that $\theta_{\rm SH}$ and the valley Seebeck signal can be greatly enhanced by vertically integrating valley Hall units, as sketched in Fig. 3(b) (right panel). In this case, the size of contact surfaces between metal leads and 2D magnets is significantly increased. By assuming that the metal leads have similar-sized thickness with the integrated valley-Hall system, we still use the typical value of $\theta_{\rm SH}$ to give estimations below.

In addition, it is assumed that the length and the width of the 2D magnet are on the order of 1 μm (see detailed estimation in Sec. V), and the temperature differences $\Delta T_{\rm L}$ in Fig. 3(a) and ΔT in Fig. 3(b) should be much lower than the basic temperature T and are on the orders of 10^{-3}–1 K, which is available with the application of current experimental techniques [44,49,50]. The measured signal can be effectively enhanced by increasing the temperature difference.

V. MATERIAL REALIZATION

Our proposal for topological valley Hall effect of magnons can be experimentally detected in a number of 2D FM insulators. One possibility is bilayer $CrBr_3$, which has an electronic band gap about 1.4 eV [51,52] and $S = 3/2$ for each Cr^{3+} ion [6]. According to experimental results [6,32,51], the Hamiltonian (1) without H_U indeed captures the intrinsic magnon physic of this material, and quantum fluctuations are not as important as that in spin 1/2 systems [8]. In addition, corrections from the single-ion magnetic anisotropy term $H_{\mathcal{A}} = \mathcal{A}\sum_{\langle i,j\rangle}(S_i^z)^2$ shift up the magnon bands by a small energy $2\mathcal{A}$ below 0.1 meV [53]. This effect is not relevant for topological transport dominated by high-energy THz magnons near two valleys.

By applying the electrostatic doping technique [54] to bilayer $CrBr_3$, the localized moments in each layer can be continually tuned (more than 20% electron or hole doping was achieved in CrI_3 [30]). For a typical doping case, the two monolayers are doped equally with opposite charges, and the localized moments in the FM ground state can be described as $\boldsymbol{S}_{i,\alpha} = (S - \alpha\Delta S)\hat{z}$. One advantage of this doping is that the variation of parameters $J_\perp$, λ in Eq. (1) can be safely ignored [30]. The $\mathcal{I}$ breaking term H_U has the specific form

$$H_U = \sum_i \alpha U S_i^z \quad \text{with} \quad U = \Delta S. \tag{11}$$

The doping also creates interlayer electric field. However, we expect that it has a minor contribution to ΔS [29] because the two insulating layers are weakly coupled.

Figure 4 shows the results of the calculation of $\kappa_{xy}^{\rm v}$ for bilayer $CrBr_3$ for different U and T. They indicate that $\kappa_{xy}^{\rm v}$ is lower than 0.1 mW/m K below 12 K because the Berry curvature for the dominant low-energy magnons away from two valleys is nearly zero (Fig. 2). Near $T = 30$ K (Curie

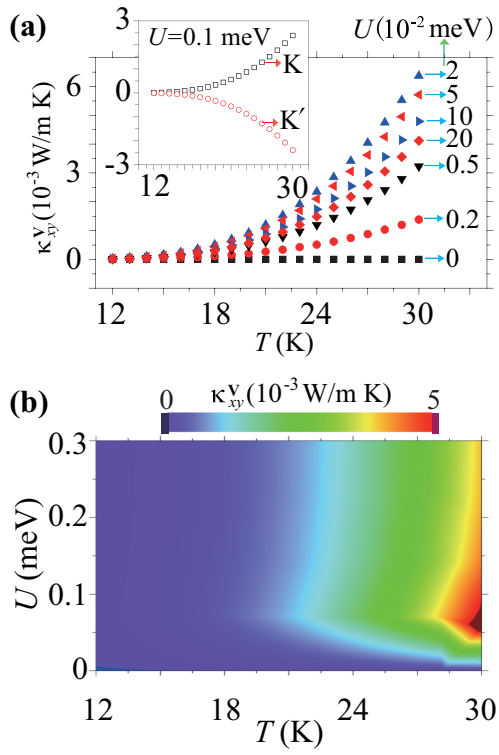

FIG. 4. Valley Hall conductivity (a) as a function of temperature under the influence of U and (b) in the (U, T) plane. The other parameters are taken from $CrBr_3$ (see the caption in Fig. 1).

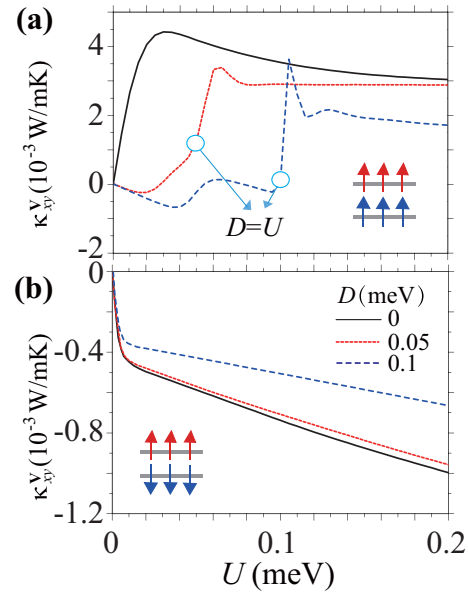

FIG. 5. Valley Hall conductivity as a function of potential U under the influence of DMI in (a) FM and (b) LAF samples at $T = 28$ K. The solid, dot, and dashed lines represent the results of $D = 0, 0.05, 0.1$ in units of meV, respectively. The other parameters from $CrBr_3$ in Fig. 1 are taken. Pure valley current $\kappa^K_{xy} = -\kappa^{K'}_{xy}$ [40] is only present for $D = 0$ in both (a) and (b).

temperature $T_C = 34$ K [32]), κ^v_{xy} can exceed 6 mW/m K, which is about one order of magnitude greater than the Hall signal reported in 3D FM insulators [43] demonstrating the advantage of Dirac magnons here. We assume a typical value of $\kappa_{xy}/\kappa_{xx} \sim 5 \times 10^{-3}$ (see SM [40], where κ_{xx} contributed from electrons, phonons, and magnons are discussed), which agrees with the latest experimental detection in other 2D magnets [49,55]. By fixing $L = 4W = 2\ell_v$ ($\ell_v \sim 1.0$ μm is expected from valleytronic experiments [21–23]), ρ_{NL} is estimated from Eq. (9) to be about 4×10^{-6} mK/W which in principle is experimentally detectable [46]. The ISH voltage in Fig. 4 is estimated from Eq. (10) as $V_{ISH} \sim 0.06$ μV/K (SM [40]) by using the typical parameters [46] $\theta_{SH} = 0.0037$, $\rho = 0.91$ $\mu\Omega$ m in Pt. Above T_C, the detection signal should decrease drastically due to the enhanced magnetic disorder [43].

Permitted by symmetry in hexagonal structure, there may exist the Dzyaloshinskii-Moriya interaction (DMI) [7,25,56], $H_{DM} = [D/(3\sqrt{3})] \sum_{\langle\langle ij \rangle\rangle} \nu_{ij} \hat{\mathbf{z}} \cdot (\boldsymbol{S}_i \times \boldsymbol{S}_j)$ with $\nu_{ij} = +1\,(-1)$ if the exchange between two next-nearest spins is clockwise (anticlockwise). DMI can induce magnon Hall effect [25] by breaking $\mathcal{T}$ but does not generate topological difference between two valleys. To clarify the influence of DMI, we calculate κ^v_{xy} as a function of U in Fig. 5(a) for $D = 0,\ 0.05,\ 0.1$ meV. As expected, κ^v_{xy} becomes weaker under the effect of DMI, and can be enhanced by increasing U. Near the circled points $D = U$, the gap closing and reopening near one valley occur (SM [40]), and κ_{xy} changes drastically due to the sign change of Berry curvature.

Moreover, we consider the influence of layered antiferromagnetic (LAF) order [31], which means each layer is FM while the FM orientation is opposite between two layers. For the LAF system, H_U in Eq. (1) should be replaced by $H_U = U \sum_i S^z_i$ (in the ground state, S^z_i is opposite for two layers). The results shown in Fig. 5(b) indicate that the layer polarity term H_U is still useful to strengthen the signal of κ^v_{xy}, reaching 1 mW/mK at $T = 28$ K for a weaker DMI. Compared with the FM bilayer case, the almost opposite Berry curvature [25,40] of magnon bands for the LAF case hinders the enhancement of topological valley current. To induce H_U, the perpendicular magnetic field [29] is feasible besides doping. As U increases, a transition of LAF to FM [29] should happen, and a stronger topological valley signal is detectable.

VI. DISCUSSION AND CONCLUSIONS

The picture of topological valley transport of magnons discussed in bilayer $CrBr_3$ also applies to multilayer FM $CrBr_3$ [32,35,36], bilayer or multilayer $CrBr_xI_{3-x}$ [53], or CrI_3 [30]. A particular issue is the Gilbert damping [18], for which the damping constant in the Landau-Lifshitz-Gilbert equation is estimated as 10^{-4} [49,55–57] under the effects of the weak Rashba-type DMI (an interaction between nearest neighbors of localized spins [56]) or disorder. The Gilbert damping usually affects the magnon-related transport properties by determining the magnon lifetime [44,58], and might be weakened by improving the sample quality and optimizing the sample scales. This damping and our proposed effects are expected to change little in the weak doping case $U \ll J$ we focus on (the system can preserve insulating properties

by adjusting gates). However, if the doped magnet becomes metallic, the localized spin model alone probably does not work. Additional significant effects to influence the magnon valley Hall effect should be considered due to the interaction between magnons and electrons/holes. It is still an open question that whether more complicated mechanisms work for larger U or a doping-induced metallic case. Certainly it is promising in view of an application to apply the physics discussed here to other 2D FM insulators with higher Curie temperature.

We now discuss DMI interactions. On one hand, the DMI parameter D (Fig. 5) in the two layers of the bilayer system are considered to be of the same sign, because this DMI interaction between next-nearest neighbors of localized spins originates from the atomic spin-orbit couplings [7,35,53] and is determined by the atomic structure of the crystal. Further calculations indicate that, when D in the two layers take the opposite sign, the signal of κ^{v}_{xy} cannot be stronger than that in the case of $D = 0$. On the other hand, the Rashba-type DMI may be enhanced at some interfaces between the magnet and its coupled proximity materials, by van der Waals engineering [4] or by increasing an out-of-plane electric field [56]. If the Rashba DMI is strong enough (approximately exceeding J_z), the magnon valley Hall transport is significantly modulated due to the topological phase transitions of energy bands, as demonstrated in similar electronic systems based on bilayer graphene [59,60].

Moreover, it is still necessary to clarify the following two points. First, for the 2D bulk system we consider, there is no anisotropy because the magnon Hall effect is dominated by the bulk states that are basically isotropic (as shown by the magnon bands near two valleys in Fig. 1). Furthermore, the result $\kappa^{\mathrm{v}}_{yx} = \kappa^{\mathrm{v}}_{xy}$ (by switching x and y in calculations) proves this point. However, for narrow nanoribbons with zigzag and armchair edges, the anisotropy of magnon valley Hall conductivity cannot be ignored due to the quantum confinement effect, as also happens in the electronic case [61]. Second, inelastic many-body interactions between magnons should be considered when the basic temperature T of the system approaches T_{C}. According to the results of Ref. [6], the many-body interactions in crystal would renormalize the magnon bands (the strength of the renormalization depends on temperature), but however would not alter the symmetries of the system. In this sense, the symmetry-protected phenomenon of topological valley transport of magnons is robust.

In summary, we have shown that THz magnons are an attractive platform for valleytronics beyond fermions and form the basis for valley-controlled magnonic applications. Our results will motivate the experimental exploration of valley-related magnon physics in 2D van der Waals magnets. Richer valley properties of topology and transport can be expected under the combined effect of magnetic order, symmetry breaking, and magnetic interactions.

ACKNOWLEDGMENTS

We thank T. Yu and G. E. W. Bauer for helpful discussions. The work was supported by the National Natural Science Foundation of China with Grant No. 61874057, the QingLan Project of Jiangsu Province (2019), the 1311 Talent Program "DingXin Scholar" of NJUPT (2018), and the Jiangsu Government Scholarship for Overseas Studies.

[1] C. Gong, L. Li, Z. Li, H. Ji, A. Stern, Y. Xia, T. Cao, W. Bao, C. Wang, Y. Wang, Z. Q. Qiu, R. J. Cava, S. G. Louie, J. Xia, and X. Zhang, Nature (London) **546**, 265 (2017).

[2] B. Huang, G. Clark, E. Navarro-Moratalla, D. R. Klein, R. Cheng, K. L. Seyler, D. Zhong, E. Schmidgall, M. A. McGuire, D. H. Cobden, W. Yao, D. Xiao, P. Jarillo-Herrero, and X. Xu, Nature (London) **546**, 270 (2017).

[3] K. S. Burch, D. Mandrus, and J.-G. Park, Nature (London) **563**, 47 (2018).

[4] C. Gong and X. Zhang, Science **363**, eaav4450 (2019).

[5] M. Gibertini, M. Koperski, A. F. Morpurgo, and K. S. Novoselov, Nat. Nanotechnol. **14**, 408 (2019).

[6] S. S. Pershoguba, S. Banerjee, J. C. Lashley, J. Park, H. Ågren, G. Aeppli, and A. V. Balatsky, Phys. Rev. X **8**, 011010 (2018).

[7] L. Chen, J.-H. Chung, B. Gao, T. Chen, M. B. Stone, A. I. Kolesnikov, Q. Huang, and P. Dai, Phys. Rev. X **8**, 041028 (2018).

[8] R. Cheng, S. Okamoto, and D. Xiao, Phys. Rev. Lett. **117**, 217202 (2016).

[9] A. Rycerz, J. Tworzydło, and C. W. J. Beenakker, Nat. Phys. **3**, 172 (2007).

[10] K. F. Mak, K. L. McGill, J. Park, and P. L. McEuen, Science **344**, 1489 (2014).

[11] X. Xu, W. Yao, D. Xiao, and T. F. Heinz, Nat. Phys. **10**, 343 (2014).

[12] H. Pan, Z. Li, C.-C. Liu, G. Zhu, Z. Qiao, and Y. Yao, Phys. Rev. Lett. **112**, 106802 (2014).

[13] Z. Niu, New J. Phys. **21**, 093044 (2019).

[14] J. R. Shaibely, H. Yu, G. Clark, P. Rivera, J. S. Ross, K. L. Seyler, W. Yao, and X. Xu, Nat. Rev. Mater. **1**, 16055 (2016).

[15] S. A. Vitale, D. Nezich, J. O. Varghese, P. Kim, N. Gedik, P. Jarillo-Herrero, D. Xiao, and M. Rothschild, Small **14**, 1801483 (2018).

[16] J. Noh, S. Huang, K. P. Chen, and M. C. Rechtsman, Phys. Rev. Lett. **120**, 063902 (2018).

[17] J. Lu, C. Qiu, W. Deng, X. Huang, F. Li, F. Zhang, S. Chen, and Z. Liu, Phys. Rev. Lett. **120**, 116802 (2018).

[18] A. V. Chumak, V. I. Vasyuchka, A. A. Serga, and B. Hillebrands, Nat. Phys. **11**, 453 (2015).

[19] W. Jin, H. H. Kim, Z. Ye, S. Li, P. Rezaie, F. Diaz, S. Siddiq, E. Wauer, B. Yang, C. Li, S. Tian, K. Sun, H. Lei, A. W. Tsen, L. Zhao, and R. He, Nat. Commun. **9**, 5122 (2018).

[20] D. Xiao, W. Yao, and Q. Niu, Phy. Rev. Lett. **99**, 236809 (2007).

[21] Y. Shimazaki, M. Yamamoto, I. V. Borzenets, K. Watanabe, T. Taniguchi, and S. Tarucha, Nat. Phys. **11**, 1032 (2015).

[22] M. Sui, G. Chen, L. Ma, W.-Y. Shan, D. Tian, K. Watanabe, T. Taniguchi, X. Jin, W. Yao, D. Xiao, and Y. Zhang, Nat. Phys. **11**, 1027 (2015).

[23] R. V. Gorbachev, J. C. W. Song, G. L. Yu, A. V. Kretinin, F. Withers, Y. Cao, A. Mishenko, I. V. Grigorieva, K. S.

Novoselov, L. S. Levitov, and A. K. Geim, Science **346**, 448 (2014).
[24] V. A. Zyuzin and A. A. Kovalev, Phys. Rev. Lett. **117**, 217203 (2016).
[25] S. A. Owerre, Phys. Rev. B **94**, 094405 (2016).
[26] D. Xiao, M.-C. Chang, and Q. Niu, Rev. Mod. Phys. **82**, 1959 (2010).
[27] Z. Wu, B. T. Zhou, X. Cai, P. Cheung, G.-B. Liu, M. Huang, J. Lin, T. Han, L. An, Y. Wang, S. Xu, G. Long, C. Cheng, K. T. Law, F. Zhang, and N. Wang, Nat. Commun. **10**, 611 (2019).
[28] J. Lee, K. F. Mak, and J. Shan, Nat. Nanotechnol. **11**, 421 (2016).
[29] S. Jiang, J. Shan, and K. F. Mak, Nat. Mater. **17**, 406 (2018).
[30] S. Jiang, L. Li, Z. Wang, K. F. Mak, and J. Shan, Nat. Nanotechnol. **13**, 549 (2018).
[31] W. Chen, Z. Sun, Z. Wang, L. Gu, X. Xu, S. Wu, and C. Gao, Science **366**, 983 (2019).
[32] Z. Zhang, J. Shang, C. Jiang, A. Rasmita, W. Gao, and T. Yu, Nano Lett. **19**, 3138 (2019).
[33] S. A. Owerre, J. Phys.: Condens. Matter **28**, 386001 (2016).
[34] H. Suzuura and T. Ando, Phys. Rev. Lett. **89**, 266603 (2002).
[35] M. A. McGuire, Crystals **7**, 121 (2017).
[36] N. Richter, D. Weber, F. Martin, N. Singh, U. Schwingenschlögl, B. V. Lotsch, and M. Kläui, Phys. Rev. Mater. **2**, 024004 (2018).
[37] E. McCann, Phys. Rev. B **74**, 161403(R) (2006).
[38] J. H. van Vleck, Phys. Rev. **33**, 467 (1929).
[39] P.-O. Löwdin, J. Chem. Phys. **19**, 1396 (1951).
[40] See Supplemental Material at http://link.aps.org/supplemental/10.1103/PhysRevB.102.075407 for details on the derivations of Eqs. (5) and (9), the calculations of thermal conductivity in Figs. 1–3, the estimation from Eq. (10), and the discussion for edge states.
[41] H. Katsura, N. Nagaosa, and P. A. Lee, Phys. Rev. Lett. **104**, 066403 (2010).
[42] J. H. Han and H. Lee, J. Phys. Soc. Jap. **86**, 011007 (2017).
[43] Y. Onose, T. Ideue, H. Katsura, Y. Shiomi, N. Nagaosa, and Y. Tokura, Science **329**, 297 (2010).
[44] G. E. W. Bauer, E. Saitoh, and B. J. van Wees, Nat. Mater. **11**, 391 (2012).
[45] D. A. Abanin, A. V. Shytov, L. S. Levitov, and B. I. Halperin, Phys. Rev. B **79**, 035304 (2009).
[46] K. Uchida, J. Xiao, H. Adachi, J. Ohe, S. Takahashi, J. Ieda, T. Ota, Y. Kajiwara, H. Umezawa, H. Kawai, G. E. W. Bauer, S. Maekawa, and E. Saitoh, Nat. Mater. **9**, 894 (2010).
[47] X. Li, B. Fauqué, Z. Zhu, and K. Behnia, Phys. Rev. Lett. **124**, 105901 (2020).
[48] L. J. Cornelissen, K. J. H. Peters, G. E. W. Bauer, R. A. Duine, and B. J. van Wees, Phys. Rev. B **94**, 014412 (2016).
[49] W. Xing, L. Qiu, X. Wang, Y. Yao, Y. Ma, R. Cai, S. Jia, X. C. Xie, and W. Han, Phys. Rev. X **9**, 011026 (2019).
[50] T. Liu, J. Peiro, D. K. de Wal, J. C. Leutenantsmeyer, M. H. D. Guimarães, and B. J. van Wees, Phys. Rev. B **101**, 205407 (2020).
[51] L. Webster and J.-A. Yan, Phys. Rev. B **98**, 144411 (2018).
[52] H. Wang, V. Eyert, and U. Schwingenschlögl, J. Phys.: Condens. Matter **23**, 116003 (2011).
[53] M. Abramchuk, S. Jaszewski, K. R. Metz, G. B. Osterhoudt, Y. Wang, K. S. Burch, and F. Tafti, Adv. Mater. **30**, 1801325 (2018).
[54] C. H. Ahn, A. Bhattacharya, M. Di Ventra, J. N. Eckstein, C. D. Frisbie, M. E. Gershenson, A. M. Goldman, I. H. Inoue, J. Mannhart, A. J. Millis, A. F. Morpurgo, D. Natelson, and J.-M. Triscone, Rev. Mod. Phys. **78**, 1185 (2006).
[55] X. S. Wang and X. R. Wang, J. Phys. D: Appl. Phys. **51**, 194001 (2018).
[56] S. K. Kim, H. Ochoa, R. Zarzuela, and Y. Tserkovnyak, Phys. Rev. Lett. **117**, 227201 (2016).
[57] A. A. Pervishko, M. I. Baglai, O. Eriksson, and D. Yudin, Sci. Rep. **8**, 17148 (2018).
[58] A. Rückriegel, A. Brataas, and R. A. Duine, Phys. Rev. B **97**, 081106(R) (2018).
[59] Y. Ren, Z. Qiao, and Q. Niu, Rep. Prog. Phys. **79**, 066501 (2016).
[60] X. Zhai and G. Jin, Phys. Rev. B **93**, 205427 (2016).
[61] X. Zhai and Y. M. Blanter, Phys. Rev. B **101**, 155425 (2020).